JACS
JOURNAL OF THE AMERICAN CHEMICAL SOCIETY

Communication

pubs.acs.org/JACS

Endohedral Metal-Induced Regioselective Formation of Bis-Prato Adduct of $Y_3N@I_h$-C_{80} and $Gd_3N@I_h$-C_{80}

Safwan Aroua,[†] Marc Garcia-Borràs,[‡] Marc Florian Bölter,[†] Sílvia Osuna,*[,‡] and Yoko Yamakoshi*[,†]

[†]Laboratorium für Organische Chemie, ETH-Zürich, Vladimir-Prelog-Weg 3, CH-8093 Zürich, Switzerland

[‡]Institut de Química Computacional i Catàlisi (IQCC) and Departament de Química, Universitat de Girona, Campus Montilivi, 17071 Girona, Catalonia, Spain

Supporting Information

ABSTRACT: Regioselective bisaddition of $M_3N@I_h$-C_{80} (M = Y, Gd) was observed for the first time in the Prato reaction with *N*-ethylglycine and formaldehyde. The main kinetic bisadduct of $Y_3N@C_{80}$ was determined to be a [6,6],[6,6] adduct by ^1H and ^{13}C NMR and vis/NIR spectroscopy, and it converted to a mixture of regioisomers upon heating via a sigmatropic rearrangement. The main kinetic bisadduct of $Gd_3N@C_{80}$ (the [6,6],[6,6] adduct on the basis of vis/NIR data) existed stably under thermal conditions without isomerization. The likely position of the second addition of the $Gd_3N@C_{80}$ bisadduct was predicted by DFT calculations.

Because of the increasing attention devoted to metallofullerenes, especially to the trimetallic nitride template endohedral metallofullerenes (TNT-EMFs, e.g., $M_3N@I_h$-C_{80}, denoted as $M_3N@C_{80}$),[1] as functional moieties for materials such as photovoltaic devices[2] and magnetic resonance imaging contrast agents (MRI-CAs),[3] controlled chemical functionalization methods for TNT-EMFs have become very important. Suitable methods for the covalent functionalization of $M_3N@C_{80}$ were previously reported, including Diels–Alder reaction,[4a] Bingel–Hirsch reaction,[4b] silylation,[4c] [2 + 2] cycloaddition,[4d] electrochemical reaction,[4e] azide addition,[4f] and Prato 1,3-dipolar cycloaddition.[4g,h] The Prato reaction, which was initially reported as a derivatization method for C_{60},[5] provides stable adducts of $M_3N@C_{80}$ in reasonable yields and has been highly used in the preparations of new fullerene derivatives. The intensive studies of the $M_3N@C_{80}$ Prato reaction, especially by the groups of Echegoyen and Dorn, indicated that the initial Prato addition generally occurs on the [6,6] bond (between two hexagons) of C_{80} and subsequently rearranges to the [5,6] junction (between a pentagon and a hexagon). In our previous reports, we found that this [6,6]-to-[5,6] rearrangement is in equilibrium when larger endohedral metals (e.g., M = Y, Gd) are present because of the low energy difference between the [6,6] and [5,6] adducts.[6,7] Although monofunctionalization of $M_3N@C_{80}$ was well-studied as described above, there are few reports on the bisaddition, except for the Bingel cyclopropanation of $Sc_3N@C_{78}$, the carbene addition of $La_2@C_{80}$, and cycloaddition to $La@C_{72}(C_6H_3Cl_2)$.[8−10] In this study, we investigated the Prato bisaddition reaction of $M_3N@C_{80}$ (M = Sc, Lu, Y, Gd) using a dipole with a small N-substituent (*N*-ethylazomethine ylide). We found that bisadducts were easily generated in the presence of larger metal clusters such as Y_3N and Gd_3N. Very interestingly, in both $Y_3N@C_{80}$ and $Gd_3N@C_{80}$, the second addition kinetically occurred in a regioselective manner to provide one major isomer of the [6,6],[6,6] bisadduct. Upon subsequent thermal treatment, the initial regioselective bisadduct of $Y_3N@C_{80}$ was converted to a mixture of isomers via rearrangement, while no significant isomerization of the major kinetic bisadduct of $Gd_3N@C_{80}$ was observed.

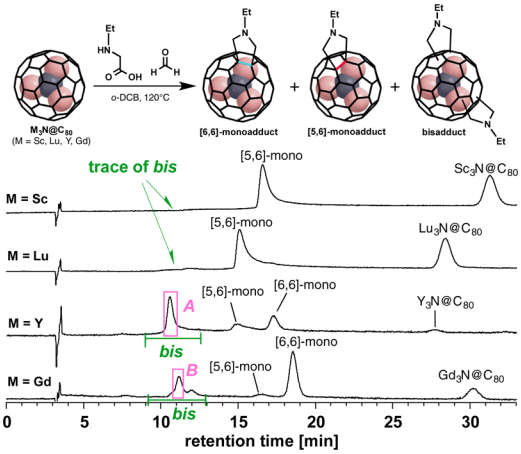

Figure 1. Prato reactions of $M_3N@C_{80}$ and regioselective generation of bisadducts (peak A for $Y_3N@C_{80}$ and peak B for $Gd_3N@C_{80}$). Reaction conditions: *N*-ethylglycine (8.5 equiv) and formaldehyde (45 equiv) in *o*-DCB at 120 °C for 1 h. HPLC: Buckyprep (4.6 mm × 250 mm), toluene 1.0 mL/min, 390 nm.

Prato reactions of $M_3N@C_{80}$ (M = Sc, Lu, Y, Gd) were carried out under consistent conditions in the presence of *N*-ethylglycine (8.5 equiv) and formaldehyde (45 equiv) in *o*-dichlorobenzene (*o*-DCB) at 120 °C for 1 h (Figure 1). The reaction processes were monitored by HPLC using a Buckyprep column. Under these conditions, significant amounts of bisadducts were generated in the reactions of $Y_3N@C_{80}$ and $Gd_3N@C_{80}$, while only the monoadducts ([5,6] adducts that were converted from the initially formed [6,6] adducts) and minor traces of bisadducts were observed in the reactions of $Sc_3N@C_{80}$ and $Lu_3N@C_{80}$. No significant amounts of $Sc_3N@C_{80}$ bisadducts were observed even in the presence of 17 equiv of *N*-ethylglycine (Figure S3 in the Supporting Information (SI)).

Received: October 26, 2014
Published: December 24, 2014

DOI: 10.1021/ja511008z
J. Am. Chem. Soc. 2015, 137, 58−61

As indicated in HPLC analyses, the bisadducts of both $Y_3N@C_{80}$ and $Gd_3N@C_{80}$ were generated in a regioselective manner with major peaks A and B (Figure 1). Each isolated product A and B showed a single peak in two additional HPLC analyses using Buckyprep-M and PBB columns (Figures S5 and S15), indicating that each peak A and B presumably consisted of a single isomer. Further characterizations of peaks A and B were carried out using vis/NIR spectroscopy (Figure 2), MALDI-TOF mass spectrometry (Figures S12 and S17), and ^{1}H and ^{13}C NMR spectroscopy (only for peak A; Figure 3) for structure elucidation.

Figure 2 shows the vis/NIR spectra of the main bisadducts of $Y_3N@C_{80}$ (peak A in Figure 1) and $Gd_3N@C_{80}$ (peak B in Figure

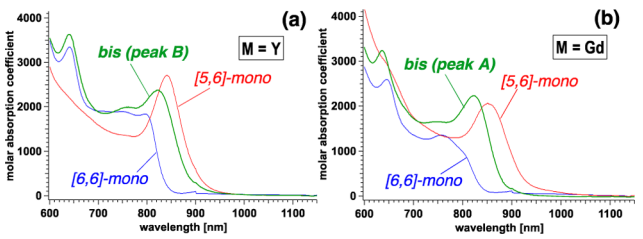

Figure 2. Vis/NIR spectra of isolated peaks (a) A and (b) B of the bisadducts of $Y_3N@C_{80}$ and $Gd_3N@C_{80}$ (in toluene). The [6,6] and [5,6] monoadducts with a bis(*tert*-butoxycarbonyl) group[6] were used as standard compounds (monoadducts of *N*-ethylfulleropyrrolidines of $M_3N@C_{80}$ were not soluble enough in toluene for vis/NIR analysis).

1). By comparison with the previously reported characteristic vis/NIR spectra of the [6,6] and [5,6] monoadducts of $M_3N@C_{80}$ (typically three bands for [6,6] adducts and one band for [5,6] adducts),[4d,6,7] the regioselectively obtained main bisadducts of $Y_3N@C_{80}$ and $Gd_3N@C_{80}$ were both suggested to be [6,6],[6,6] bisadducts. This was further confirmed for the $Y_3N@C_{80}$ bisadduct by ^{1}H and ^{13}C NMR spectroscopy as described below (peak B was paramagnetic).

In the ^{1}H NMR spectrum (Figure 3a), four pairs of methylene protons from the pyrrolidine groups (a total of eight doublets, H^{1-4A} and H^{1-4B}) and two pairs of methylene protons from the ethyl groups (two quartets, H^5, H^6) were observed, suggesting that the isolated peak A contained a single isomer of an unsymmetrical bisadduct. This was further confirmed by the ^{13}C NMR spectrum (Figure 3b), with 76 peaks corresponding to the sp^2 carbons of the C_{80} cage (in the region of 105−155 ppm). Consistent with the vis/NIR analyses, both addition sites of the $Y_3N@C_{80}$ bisadduct were confirmed to be on [6,6] junctions on the basis of the ^{13}C NMR chemical shifts of C^{9AB} and C^{11AB} observed downfield at 130−145 ppm (in [5,6] adducts, sp^2 cage carbons adjacent to the sp^3 addition site should be observed upfield at 105−120 ppm).[6,11]

The multiple HPLC analyses together with the vis/NIR and NMR spectra clearly confirmed that peak A contained a single regioisomer of an unsymmetric [6,6],[6,6] bisadduct of $Y_3N@C_{80}$ and that the second Prato addition proceeded in a highly regioselective manner. Since the bis-Prato adducts of C_{60} are generally obtained in a non-regioselective manner when tether chemistry is not used,[12,13] this highly regioselective second addition of the dipole to the C_{80} cage is speculated to be due to the effect of the metallic cluster inside C_{80}. Since the addition sites of the main bisadducts were both on [6,6] junctions, the second addition seemed to occur only on the [6,6] monoadduct before it was converted to the [5,6] monoadduct. To experimentally demonstrate this, the reactivities of the [6,6] and [5,6] monoadducts of $Y_3N@C_{80}$ against the second Prato

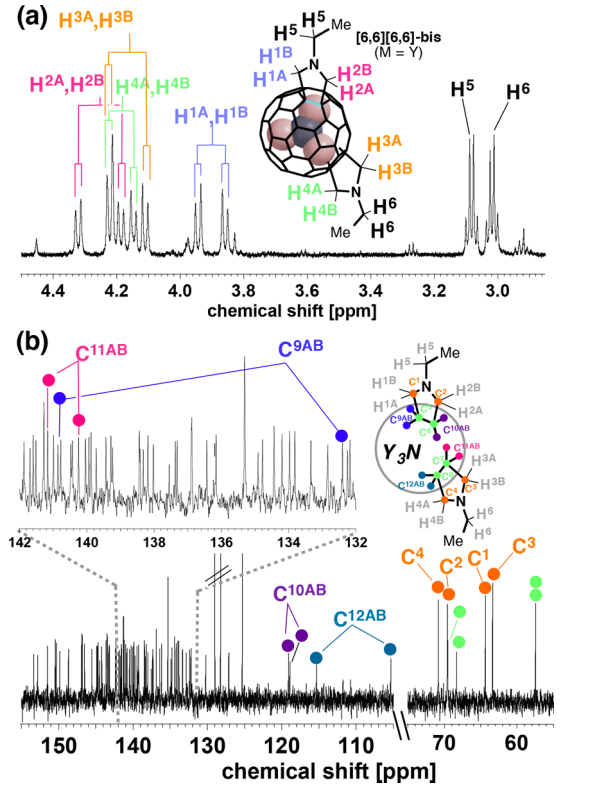

Figure 3. (a) ^{1}H and (b) ^{13}C NMR spectra of the $Y_3N@C_{80}$ bisadduct (peak A) in 1:1 $CDCl_3/CS_2$. Assignments were based on the ^{1}H−^{1}H COSY, HSQC, and HMBC measurements (Figures S9−S11).

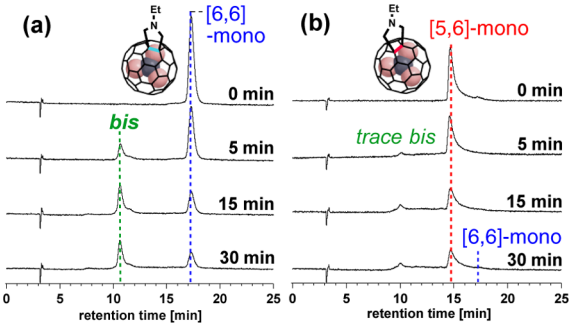

Figure 4. Second Prato reactions with the (a) [6,6] and (b) [5,6] monoadducts of $Y_3N@C_{80}$. Conditions: *N*-ethylglycine (5.0 equiv) and formaldehyde (45 equiv) in *o*-DCB at 120 °C. The bisadduct was observed significantly only in the reaction with the [6,6] monoadduct. HPLC conditions as in Figure 1.

reaction were compared (Figures 4 and S13). While the second Prato addition to the [6,6] adduct occurred efficiently (Figure 4a), much lower production of the bisadduct was observed in the reaction of the [5,6] adduct (Figure 4b). This result is in line with the fact that very small amounts of bisadducts were observed in the reactions of $Sc_3N@C_{80}$ and $Lu_3N@C_{80}$ (Figure 1), where the [6,6]-to-[5,6] isomerization of the monoadducts proceeeded too fast for the second Prato addition to occur.

On the basis of previous studies, we expected that the relative positions of bis-Prato addition could relocate upon thermal treatment via a sigmatropic rearrangement. We subjected the main kinetic bisadducts of $Y_3N@C_{80}$ and $Gd_3N@C_{80}$ to thermal conditions. *o*-DCB solutions of the isolated kinetic bisadducts (peaks A and B in Figure 1) were kept at 130 °C, and the reaction

DOI: 10.1021/ja511008z
J. Am. Chem. Soc. 2015, 137, 58−61

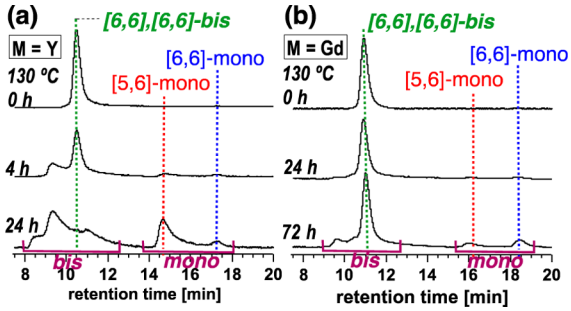

Figure 5. Thermal treatment of the major bisadducts of (a) $Y_3N@C_{80}$ (peak A in Figure 1) and (b) $Gd_3N@C_{80}$ (peak B in Figure 1) at 130 °C in *o*-DCB. HPLC conditions as in Figure 1.

processes were monitored by HPLC (Figures 5 and S19). After 4 h, the single peak of the main bisadduct of $Y_3N@C_{80}$ (peak A) became a mixture of several bisadducts, and subsequent generation of monoadducts via retro-cycloaddition[14] was observed after 4 h (Figure 5a). After 24 h, the kinetic bisadduct mostly disappeared, giving a mixture of various bisadducts and [6,6] and [5,6] monoadducts. In contrast, the same thermal treatment of the main kinetic $Gd_3N@C_{80}$ bisadduct (peak B) provided very little generation of products either from isomerization or retro-cycloaddition even after 72 h (Figure 5b). This result indicated that the kinetic [6,6],[6,6] bisadduct of $Gd_3N@C_{80}$ did not isomerize and was thermodynamically stable. It was thermally much stabler even than the $Gd_3N@C_{80}$ [6,6] monoadduct (the [6,6]-to-[5,6] isomerization of $Gd_3N@C_{80}$ monoadduct occurred with $t_{1/2}$ = 6.7 h at 120 °C).[7]

Although the spectroscopic data indicated that the kinetic bisadduct of $Y_3N@C_{80}$ was an unsymmetric [6,6],[6,6] bisadduct, this information was not sufficient to determine the exact position of the second addition site of $M_3N@C_{80}$ (M = Y, Gd). Therefore, density functional theory (DFT) calculations at the BP86-D2/TZP//BP86-D2/DZP level using the computational package ADF[15,16] were employed to estimate the thermodynamically most favorable bisaddition site of $Gd_3N@C_{80}$, taken together with the experimental observation that the kinetic bisadduct of $Gd_3N@C_{80}$ was also the thermodynamic product. A simpler *N*-methylfulleropyrrolidine was used to reduce the computational complexity, and 23 second addition sites on the C_{80} cage were considered (Figure 6a).[17] The obtained relative stabilities of the $Gd_3N@C_{80}$ bisadducts are represented as blue or black non-italic numbers (red italic numbers indicate the positions of the second addition sites). As a result, three thermodynamically preferred bisadducts of $Gd_3N@C_{80}$ were found: two [6,6],[6,6] bisadducts (marked in blue in Figure 6a) with second addition sites of 57−58 (lowest energy) and 20−22 (0.8 kcal/mol higher than 57−58) and one [6,6], [5,6] bisadduct with a second addition site of 16−20 (0.6 kcal/mol higher than 57−58). There were also three bisadducts with relative stabilities in the range of 1.2−1.8 kcal/mol.

The computed thermodynamic stabilities together with the experimental observations lead to the following conclusions. For $Gd_3N@C_{80}$, the only addition site that could lead to stable bisadducts corresponds to 57−58, which is the most favorable addition site (Figure 6a). The other thermodynamically stable [6,6],[6,6] bisadduct at 20−22 was also approximately as stable as the adjacent [5,6] bond 16−20, and therefore [6,6]-to-[5,6] isomerization would be expected. It is worth emphasizing that in the most favorable bisadducts with second addition at 57−58, both endohedral Gd atoms directly face the substituted C−C

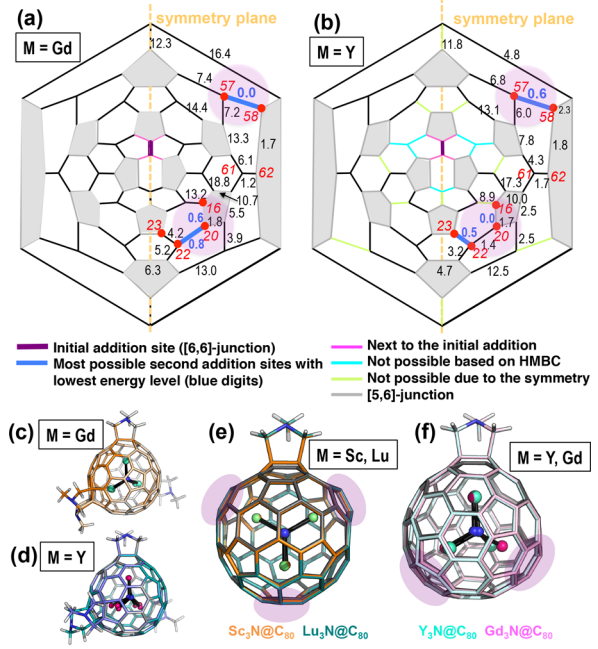

Figure 6. (a, b) Schlegel structures of (a) $Gd_3N@C_{80}$ and (b) $Y_3N@C_{80}$ with relative stabilities for 23 different bisadducts calculated at the BP86-D2/TZP//BP86-D2/DZP level of theory. Blue thick bonds represent the second addition sites of bisadducts with the lowest energies (non-italic numbers are energies in kcal/mol, red italic numbers correspond to the positions), and bonds situated close to the metal cluster are highlighted in pink. (c, d) Overlays of the lowest-energy thermodynamic [6,6],[6,6] bisadducts of (c) $Gd_3N@C_{80}$ (*16*−*20* in orange, *20*−*22* in light orange, and *57*−*58* in gray) and (d) $Y_3N@C_{80}$ (*22*−*23* in teal, *16*−*20* in blue, and *57*−*58* in gray). Larger versions are shown in Figures S21 and S22. The TNT unit is fixed in $Gd_3N@C_{80}$ but significantly rotated in $Y_3N@C_{80}$. (e, f) Superpositions of the most stable monoadducts of (e) C_{80}, $Sc_3N@C_{80}$, and $Lu_3N@C_{80}$ and (f) C_{80}, $Y_3N@C_{80}$, and $Gd_3N@C_{80}$.

bonds (Figure 6c). Interestingly, the orientations of Gd_3N in the three most favorable bisadducts were identical (Figure 6c). This indicates that the large inner metal cluster is completely fixed inside the cage after the first Prato reaction, which directs the second Prato addition toward those bonds situated in close contact. Addition to bonds close to the metal atoms is favored as they are highly pyramidalized and the fullerene cage has to be less distorted to react (see Figure 6f and Table S1 in the SI).

Similarly, DFT calculations to investigate the most favorable thermodynamic addition site for $Y_3N@C_{80}$ were carried out (Figure 6b,d). The most favorable thermodynamic second addition sites for $Y_3N@C_{80}$ were one [5,6] bond (16−20 with the lowest energy) and two [6,6] bonds (22−23 and 57−58 with stabilities of 0.5 and 0.6 kcal/mol relative to 16−20, respectively), which are shown in blue in Figure 6b. The bonds 57−58 and 22−23, which are completely surrounded by less stable [5,6] positions, could not be possible as second addition sites since no isomerization should be observed in these isomers. The obtained thermodynamic stabilities suggest that the second Prato addition to $Y_3N@C_{80}$ might be kinetically favored at the 20−22 bond, which could subsequently isomerize to the most stable 16−20 [5,6] and 22−23 [6,6] positions. We performed restrained optimizations along the reaction coordinate (linear transit (LT); Figure S20) for bonds 16−20, 20−22, and 22−23 to estimate the activation barrier for the second Prato addition in $Y_3N@C_{80}$. LT calculations indicated a slightly lower activation barrier for bond 20−22 (the relative energy of the bisadduct is 1.4

DOI: 10.1021/ja511008z
J. Am. Chem. Soc. 2015, 137, 58−61

kcal/mol) with respect to 22−23. As expected from our previous study,[7] a reactant complex (at ca. 3.4 Å) and a small activation barrier (ca. 1.0 kcal/mol) exist in the case of [5,6] addition at 16−20. From these observations, we estimate bond 20−22 to be the kinetic bisadduct site and bonds 16−20 and 22−23 as the thermodynamic bisadduct sites for $Y_3N@C_{80}$. As retro-cycloaddition was observed experimentally in the case of $Y_3N@C_{80}$, the possible addition at position 57−58 (0.6 kcal/mol) could not be discarded. Interestingly, the most stable thermodynamic $Y_3N@C_{80}$ bisadducts presented the metal cluster significantly rotated (Figure 6d). In contrast to Gd_3N, the smaller Y_3N cluster is able to rotate slightly to face the attacked C−C bond, which makes the second Prato addition less selective.

The highly favorable bisadduct formation observed in $Y_3N@C_{80}$ and $Gd_3N@C_{80}$ can be easily explained by comparison of the most stable monoadducts. It is worth emphasizing that the TNT rotation is hindered after the first functionalization even in the case of the smaller Sc and Lu clusters.[18] For monoadducts with larger metal clusters such as Y_3N and Gd_3N, one of the metal atoms directly faces the attacked bond (Figure 6f). This leads to an enhanced reactivity of those more pyramidalized areas situated close to the other two metal atoms, as shown by the computed relative stabilities. In contrast, for the cases of $Sc_3N@C_{80}$ and $Lu_3N@C_{80}$ with smaller clusters, the lowest-energy monoadducts do not present any of the metal atoms facing the attacked C−C bond (Figure 6e). This different orientation of the TNT unit directs the bisaddition to other regions of the fullerene cage. Two out of the three regions are located close to the initially functionalized bond, making the second reaction highly unfavorable because of steric repulsion. The third possible addition site is located right at the other site of the initial addition site, which should lead to highly strained bisadducts.

In summary, we have found for the first time the regioselective generation of bisadducts in the Prato reaction of $Y_3N@C_{80}$ and $Gd_3N@C_{80}$. The second addition occurred to the [6,6] monoadducts to provide [6,6],[6,6] bisadducts. While the kinetic bisadduct of $Y_3N@C_{80}$ isomerized under thermal conditions, that of $Gd_3N@C_{80}$ remained almost intact. This phenomenon could be explained by the presence of a larger metal cluster (Gd > Y), which presumably stabilizes the [6,6] monoadduct to trigger the second Prato addition and further stabilizes the [6,6],[6,6] bisadduct.

■ ASSOCIATED CONTENT

Supporting Information

Procedures, additional data, and complete ref 16. This material is available free of charge via the Internet at http://pubs.acs.org.

■ AUTHOR INFORMATION

Corresponding Authors

yamakoshi@org.chem.ethz.ch
silvia.osuna@udg.edu

Notes

The authors declare no competing financial interest.

■ ACKNOWLEDGMENTS

This research was supported in part by the Swiss National Foundation (200021-140451 and 200021-156097 to Y.Y.), ETHZ (Grant ETH-25 11-1 to Y.Y.), JST PRESTO (to Y.Y.), the American Heart Association (SDG 0930140N to Y.Y.), the Spanish MECD (Ph.D. Fellowship AP2010-2517 to M.G.-B.), Spanish MINECO (Projects CTQ2011-23156/BQU and CTQ2011-25086/BQU and Juan de la Cierva Postdoctoral Grant JCI-2012-14438 to S.O.), and the European Community (CIG Project PCIG14-GA-2013-630978 to S.O.).

■ REFERENCES

(1) Stevenson, S.; Rice, G.; Glass, T.; Harich, K.; Cromer, F.; Jordan, M. R.; Craft, J.; Hadju, E.; Bible, R.; Olmstead, M. M.; Maitra, K.; Fisher, A. J.; Balch, A. L.; Dorn, H. C. *Nature* **1999**, *402*, 898.

(2) Ross, R. B.; Cardona, C. M.; Guldi, D. M.; Sankaranarayanan, S. G.; Reese, M. O.; Kopidakis, N.; Peet, J.; Walker, B.; Bazan, G. C.; Van Keuren, E.; Holloway, B. C.; Drees, M. *Nat. Mater.* **2009**, *8*, 208.

(3) Zhang, J. F.; Fatouros, P. P.; Shu, C. Y.; Reid, J.; Owens, L. S.; Cai, T.; Gibson, H. W.; Long, G. L.; Corwin, F. D.; Chen, Z. J.; Dorn, H. C. *Bioconjugate Chem.* **2010**, *21*, 610.

(4) (a) Iezzi, E. B.; Duchamp, J. C.; Harich, K.; Glass, T. E.; Lee, H. M.; Olmstead, M. M.; Balch, A. L.; Dorn, H. C. *J. Am. Chem. Soc.* **2002**, *124*, 524. (b) Lukoyanova, O.; Cardona, C. M.; Rivera, J.; Lugo-Morales, L. Z.; Chancellor, C. J.; Olmstead, M. M.; Rodríguez-Fortea, A.; Poblet, J. M.; Balch, A. L.; Echegoyen, L. *J. Am. Chem. Soc.* **2007**, *129*, 10423. (c) Iiduka, Y.; Ikenaga, O.; Sakuraba, A.; Wakahara, T.; Tsuchiya, T.; Maeda, Y.; Nakahodo, T.; Akasaka, T.; Kako, M.; Mizorogi, N.; Nagase, S. *J. Am. Chem. Soc.* **2005**, *127*, 9956. (d) Li, F. F.; Pinzon, J. R.; Mercado, B. Q.; Olmstead, M. M.; Balch, A. L.; Echegoyen, L. *J. Am. Chem. Soc.* **2011**, *133*, 1563. (e) Li, F. F.; Rodríguez-Fortea, A.; Peng, P.; Chavez, G. A. C.; Poblet, J. M.; Echegoyen, L. *J. Am. Chem. Soc.* **2012**, *134*, 7480. (f) Liu, T. X.; Wei, T.; Zhu, S. E.; Wang, G. W.; Jiao, M. Z.; Yang, S. F.; Bowles, F. L.; Olmstead, M. M.; Balch, A. L. *J. Am. Chem. Soc.* **2012**, *134*, 11956. (g) Cardona, C. M.; Kitaygorodskiy, A.; Ortiz, A.; Herranz, M. A.; Echegoyen, L. *J. Org. Chem.* **2005**, *70*, 5092. (h) Cai, T.; Ge, Z. X.; Iezzi, E. B.; Glass, T. E.; Harich, K.; Gibson, H. W.; Dorn, H. C. *Chem. Commun.* **2005**, 3594.

(5) Prato, M.; Maggini, M.; Scorrano, G.; Lucchini, V. *J. Org. Chem.* **1993**, *58*, 3613.

(6) Aroua, S.; Yamakoshi, Y. *J. Am. Chem. Soc.* **2012**, *134*, 20242.

(7) Aroua, S.; Garcia-Borràs, M.; Osuna, S.; Yamakoshi, Y. *Chem.—Eur. J.* **2014**, *20*, 14032.

(8) Cai, T.; Xu, L.; Shu, C.; Champion, H. A.; Reid, J. E.; Anklin, C.; Anderson, M. R.; Gibson, H. W.; Dorn, H. C. *J. Am. Chem. Soc.* **2008**, *130*, 2136.

(9) Ishitsuka, M. O.; Sano, S.; Enoki, H.; Sato, S.; Nikawa, H.; Tsuchiya, T.; Slanina, Z.; Mizorogi, N.; Liu, M. T. H.; Akasaka, T.; Nagase, S. *J. Am. Chem. Soc.* **2011**, *133*, 7128.

(10) Sawai, K.; Takano, Y.; Izquierdo, M.; Filippone, S.; Martín, N.; Slanina, Z.; Mizorogi, N.; Waelchli, M.; Tsuchiya, T.; Akasaka, T.; Nagase, S. *J. Am. Chem. Soc.* **2011**, *133*, 17746.

(11) It is known that one pair of C_{80} carbons adjacent to the THJ sp^3 addition site are observed downfield for the [6, 6] adduct, while the carbons adjacent to the PHHJ sp^3 addition site are observed upfield (105−120 ppm) for both the [6,6] and [5,6] adducts.

(12) Lu, Q.; Schuster, D. I.; Wilson, S. R. *J. Org. Chem.* **1996**, *61*, 4764.

(13) Bougeois, J.-P.; Echegoyen, L.; Fibbioli, M.; Pretsch, E.; Diederich, F. *Angew. Chem., Int. Ed.* **1998**, *37*, 2118.

(14) Martin, N.; Altable, M.; Filippone, S.; Martin-Domenech, A.; Echegoyen, L.; Cardona, C. M. *Angew. Chem., Int. Ed.* **2006**, *45*, 110.

(15) Swart, M.; Bickelhaupt, F. M. *Int. J. Quantum Chem.* **2006**, *106*, 2536.

(16) Baerends, E. J.; et al. *ADF2010.1*; SCM: Amsterdam, 2010.

(17) It should be mentioned here that the reaction energies for the bisaddition in both $Y_3N@C_{80}$ and $Gd_3N@C_{80}$ were estimated to be ca. −48 kcal/mol, which are practically equivalent to the one found for the monoadduct formation (ca. −50 kcal/mol with respect to isolated reactants). These results suggest that the second addition is not affected thermodynamically by the first functionalization and is still favored.

(18) Garcia-Borràs, M.; Osuna, S.; Luis, J. M.; Swart, M.; Sola, M. *Chem.—Eur. J.* **2013**, *19*, 14931.

DOI: 10.1021/ja511008z
J. Am. Chem. Soc. 2015, 137, 58−61